Applied Physics Letters

Optimizing the spontaneous-emission of far-UVC phosphors

Cite as: Appl. Phys. Lett. **120**, 231902 (2022); https://doi.org/10.1063/5.0092109
Submitted: 21 March 2022 • Accepted: 16 May 2022 • Published Online: 06 June 2022

Ohad Segal, Avner Shultzman, Yaniv Kurman, et al.

Applied Physics Letters ARTICLE scitation.org/journal/apl

Optimizing the spontaneous-emission of far-UVC phosphors

Cite as: Appl. Phys. Lett. **120**, 231902 (2022); doi: 10.1063/5.0092109
Submitted: 21 March 2022 · Accepted: 16 May 2022 ·
Published Online: 6 June 2022

Ohad Segal,[1] Avner Shultzman,[1,2] Yaniv Kurman,[1] and Ido Kaminer[1,a)]

AFFILIATIONS

[1]Solid State Institute, Technion—Israel Institute of Technology, 32000 Haifa, Israel
[2]The Weizmann Institute of Science, 76100 Rehovot, Israel

[a)]Author to whom correspondence should be addressed: kaminer@technion.ac.il

ABSTRACT

Far-UVC light can enable virus-deactivation while remaining harmless to human tissues. This triggered great efforts to create far-UVC light sources with sufficient emission power and efficiency. However, current sources, such as mercury lamps, KrCl excimer lamps, and LEDs, are made from hazardous chemicals or are limited by low efficiency. Consequently, an alternative approach for reaching the far-UVC is now receiving renewed interest: using phosphors for converting higher frequencies to the desired range of far-UVC. However, this concept is limited by the phosphor's conversion efficiency. In this paper, we propose to utilize principles of nanophotonics to create far-UVC sources. Specifically, we design a phosphor-dielectric multilayer that increases the efficiency of far-UVC light conversion and controls the intrinsic emission properties, including the angular spectrum and emission rate, by shaping the local density of photonic states. To exemplify our approach, we design an aperiodic multilayer nanostructure made of the phosphor material $YPO_4:Pr^{3+}$, showing an increase in light extraction by a factor of 3 compared to naïve bulk structures. Our approach can be applied to any phosphor material and any emitter geometry, opening avenues for engineering nanophotonic light sources in the far-UVC and other spectral regimes.

UV lamps are a vital component for the deactivation of pathogens, such as bacteria and viruses (corona, influenza, and measles).[1] Such lamps disinfect water, air, and surfaces and are used in many medical applications.[2,3] Recently, a specific part of the far-UVC spectrum (210–235 nm) was found to be especially attractive for virus deactivation without harming exposed human tissues,[1,4] thus, manifesting the importance of far-UVC lamps.

There are several technologies today for emitting in the far-UVC spectrum, including solid-state lamps (LED-based),[5,6] KrCl excimer lamps,[7] microplasma-based lamps,[8] and mercury-vapor lamps.[9] Mercury-vapor lamps are commonly used today for disinfection; however, they emit in a harmful far-UVC wavelength (184 nm) and are made from hazardous chemicals. The other sources mentioned above emit in the safe wavelength range, but suffer from low efficiency (10%–22%)[10] compared to sources emitting in the harmful far-UVC wavelengths (such as Xe_2 excimer lamp emitting at 172 nm with an efficiency of 50%).[11] An alternate solution to emit in the essential wavelengths is to employ an efficient source at higher frequencies (such as the Xe_2 excimer lamps) and convert the spectrum using a phosphor material that emits in the far-UVC spectra.[12] This intriguing concept has so far remained limited by the phosphor's conversion efficiency.

Here, we propose a way to bypass this limit and create efficient phosphor-based far-UVC sources by using the Purcell effect to enhance the intrinsic conversion efficiency of phosphors. We introduce nanophotonic multilayer structures made of phosphors that substantially enhance the intrinsic emission rate and reshape the angular spectrum, outperforming the efficiency of existing phosphors (Fig. 1). To this end, we use constraint optimization techniques targeted at the conversion efficiency of the outcoupled far-UVC emission. Such optimization shapes the photonic local-density-of-state (LDOS), i.e., uses the Purcell effect and satisfies a high outcoupling factor.

To exemplify the concept, we designed a nanostructure that enhances the conversion efficiency by a factor of 3 with 200 nm of phosphor, divided into five layers [Fig. 1(b)]. We maximize the emission efficiency by changing the thickness of each layer in the nanostructure while fixing the total thickness of the phosphor. The resulting structures are generally aperiodic, having seemingly random layer thicknesses [Fig. 1(b)], conceptually similar to the optimized structure for nanophotonic inverse design (also referred to as topology optimization in related problems).[14] Despite the small number of layers, the nanostructures drastically improve the performance, as we also verify using finite difference time domain (FDTD) simulations. Our strategy can optimize any required figure-of-merit, depending on

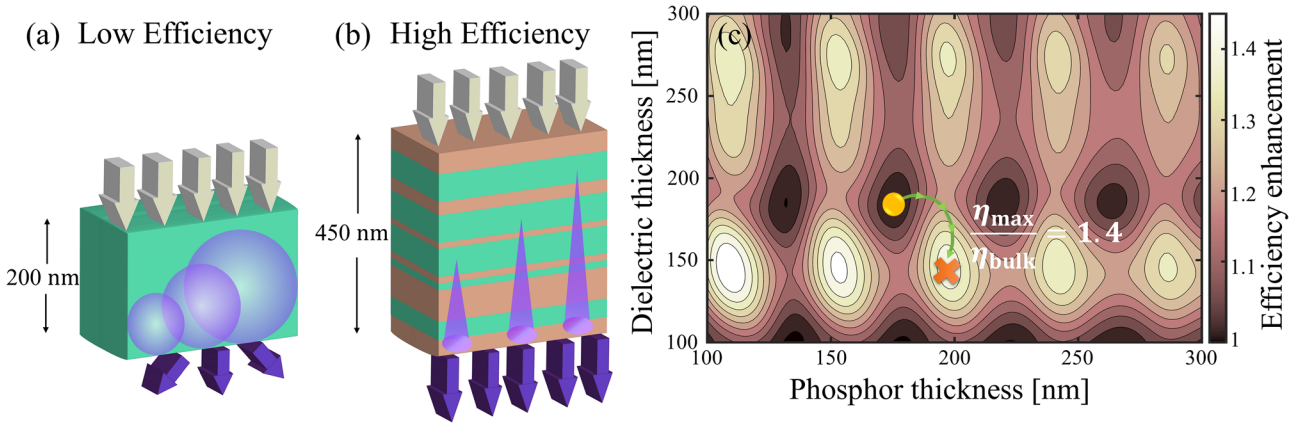

FIG. 1. Optimization of nanostructures to optimize UV emission. (a) A bulk phosphor (green), for example, YPO4:Pr3+ (refractive index 2.3),[13] converts the input radiation (gray) into far-UVC light (purple). The isotopic emission in bulk structures lowers the overall efficiency since part of the light remains trapped inside the phosphor by total internal reflection. (b) An optimized nanostructure made of layers of phosphor, and another dielectric (orange), for example, silica (index 1.6). The presented structure uses 10 layers to optimize the conversion into far-UVC light. (c) Example of the optimization process, showing the optimization map for efficiency enhancement (number of extracted UVC photons per excitation, normalized to bulk) in a two-layer nanostructure, consisting of a phosphor layer and another dielectric layer. The green path illustrates how the optimization algorithm changes the thicknesses until reaching a local optimum for the required figure-of-merit. All provided examples convert 172 nm light (e.g., from a Xe2 excimer lamp) into 235 nm in the desired band of the far-UVC.

the application, including various combinations of emission rate, directionality, and efficiency.

The Purcell effect and its generalization are the fundamental effect by which spontaneous emission can be controlled.[15–18] It describes the spontaneous emission rate enhancement of point-like localized (dipole) emitters (e.g., atoms, molecules, and quantum dots) by changing the density of states of the emitted light.[16,17] In conventional usages of the Purcell effect, the emitters are located inside a cavity with a maximized quality factor Q and a reduced light mode volume V. These factors enhance the rate of spontaneous emission by the Purcell factor F_P, which scales as Q/V. However, these design rules cannot be applied in the case studied in this work, since an efficient light outcoupling (from the device to air) requires a low Q.[19] Additionally, the points of emission are distributed over a volume that is not point-like compared to the UV wavelength, and therefore the mode volume cannot be minimized. These core differences motivate the need for a different design strategy and figure-of-merit. We develop the theory for optimizing the effective spontaneous emission enhancement, which captures the structure's global properties rather than local ones, including the structure's overall conversion efficiency. This kind of approach was first developed for enhancing scintillation from a periodic multilayer structure in Ref. 19, and a variant of this approach was also used very recently to control emission from a scintillating photonic crystal slab in Ref. 20. Our work here uses this approach with aperiodic structures, and combines it with nanophotonic optimization techniques.

We start the derivation using the formula of the spontaneous emission rate of a single dipole, under the dipole approximation[15]

$$\Gamma(\omega,\mathbf{r}_0)=\frac{2\omega}{\varepsilon_0\hbar c^2}\mathrm{Im}\left[\overleftrightarrow{G}_{\hat{p}\hat{p}}(\boldsymbol{r}_0,\boldsymbol{r}_0;\omega)\right]|\boldsymbol{p}|^2. \tag{1}$$

Here, ε_0 is the vacuum permittivity, $\hbar$ is the reduced Planck's constant, c is the speed of light in vacuum, $\hbar\omega$ is the energy difference between the ground and excited states of the dipole, and $\boldsymbol{p}$ is the dipole moment. In addition, $\boldsymbol{G}_{ij}(\mathbf{r},\mathbf{r}';\omega)$ is the dyadic Green's function, which incorporates the whole electromagnetic environment; it describes the ith component of the electric field at location $\mathbf{r}$ as a result of a dipole excitation in $\mathbf{r}'$ oriented along j. The spontaneous emission rate enhancement, that is, the Purcell factor of a local dipole, is defined by $F_P=\Gamma/\Gamma_0$, where $\Gamma_0=\Gamma_0(\omega,\mathbf{r}_0)$ is the emission rate to free space as a function of the dipole location.

In this work, we are interested in the spontaneous emission rate from a multilayered planar structure (uniform in the x–y directions) and alternating in the z-direction. As was previously shown,[19] the Green's function from any multilayered structure can be reduced into many three-layered structures with a modified reflection and transmission coefficients, where the diploe emitters are located in the central layer. We will denote the central layer as region 1, which has a thickness d and permittivity ε_1, while the lower and upper layers are denoted by regions 2 and 3, respectively, with permittivities $\varepsilon_{2,3}$. In this case, the emission rate of light outcoupling to region 3 from a single dipole averaged over all orientations, with frequency ω, and location z, is[21]

$$\begin{aligned}\Gamma(\omega,z)=\frac{\Gamma_0}{4k_1^3}\int_0^{k_3}ul_3\Bigg(&k_1^2\frac{\varepsilon_1}{\varepsilon_3}\left|\frac{T_{\|s\uparrow}(\omega,z;d)}{l_1}\exp(il_1z)\right|^2\\&+\left|T_{\|p\uparrow}(\omega,z;d)\exp(il_1z)\right|^2\\&+u^2\left|\frac{T_{\perp p\uparrow}(\omega,z;d)}{l_1}\exp(il_1z)\right|^2\Bigg)\mathrm{d}u,\end{aligned} \tag{2}$$

where k_i is the total wave vector amplitude in region i; l_i and u are the z-components and in-plane wave vector components; and $s\backslash p$ represents the TE\TM polarizations, respectively. Moreover,

$$\begin{aligned}T_{\|,s\backslash p}(\omega,z)&=\frac{t_{13,s\backslash p}\left(1+r_{12,s\backslash p}e^{2il_1(d-z)}\right)}{1-r_{12,s\backslash p}r_{13,s\backslash p}e^{2il_1d}},\\T_{\perp,s\backslash p}(\omega,z)&=\frac{t_{13,s\backslash p}\left(1-r_{12,s\backslash p}e^{2il_1(d-z)}\right)}{1-r_{12,s\backslash p}r_{13,s\backslash p}e^{2il_1d}},\end{aligned} \tag{3}$$

where r_{ij} and t_{ij} are the Fresnel's coefficients between layers $i,j \in \{1,2,3\}$. This result can be extended to a general multilayered structure using the effective Fresnel coefficients from a multilayered structure.[22] We note that using Eq. (2), we can identify the spontaneous emission rate for light outcoupling at solid angle θ, frequency ω, and location z inside the multilayer structure:

$$\gamma(\omega,\theta,\mathrm{z}) = \frac{\Gamma_0}{4}\frac{k_3 l_3^2}{k_1^3}\left(k_1^2\frac{\varepsilon_1}{\varepsilon_3}\left|\frac{T_{\parallel s}}{l_1}e^{il_1 z}\right|^2 + \left|T_{\parallel p}e^{il_1 z}\right|^2 + u^2\left|\frac{T_{\perp p}}{l_1}e^{il_1 z}\right|^2\right). \tag{4}$$

To demonstrate the effective spontaneous emission rate concept, we calculated the spontaneous emission rate according to Eq. (4) for the optimized structure presented in Fig. 1, in comparison with 200 and 450 nm bulks. In Fig. 2, we present the spontaneous emission rate for light outcoupling to free space, as a function of the emission angle, frequency, and depth inside the structures. The non-emitting dielectric layers are marked in gray. The results show how the optimized nanostructure shapes the emission rate, which achieves a unique emission pattern.

In order to visualize the contribution of each phosphor layer to the overall emission, we present in Fig. 3 the depth-dependent spontaneous emission summed over all angles and frequencies that outcouple to free space. We observe that in most of the emitting layers in the optimized structure, the emission is substantially enhanced compared to the bulk structures.

To characterize the entire nanostructure, we convert the local emission properties that depend on the depth z, to a global property: the effective angle-dependent emission rate Γ_{eff}, defined as the number of photons per second that couple out of the nanostructure, for each angle θ and frequency ω:[19]

$$\Gamma_{\mathrm{eff}}(\theta,\omega) = \int dz G(z)\gamma(\omega,\theta,\mathrm{z})Y(\omega). \tag{5}$$

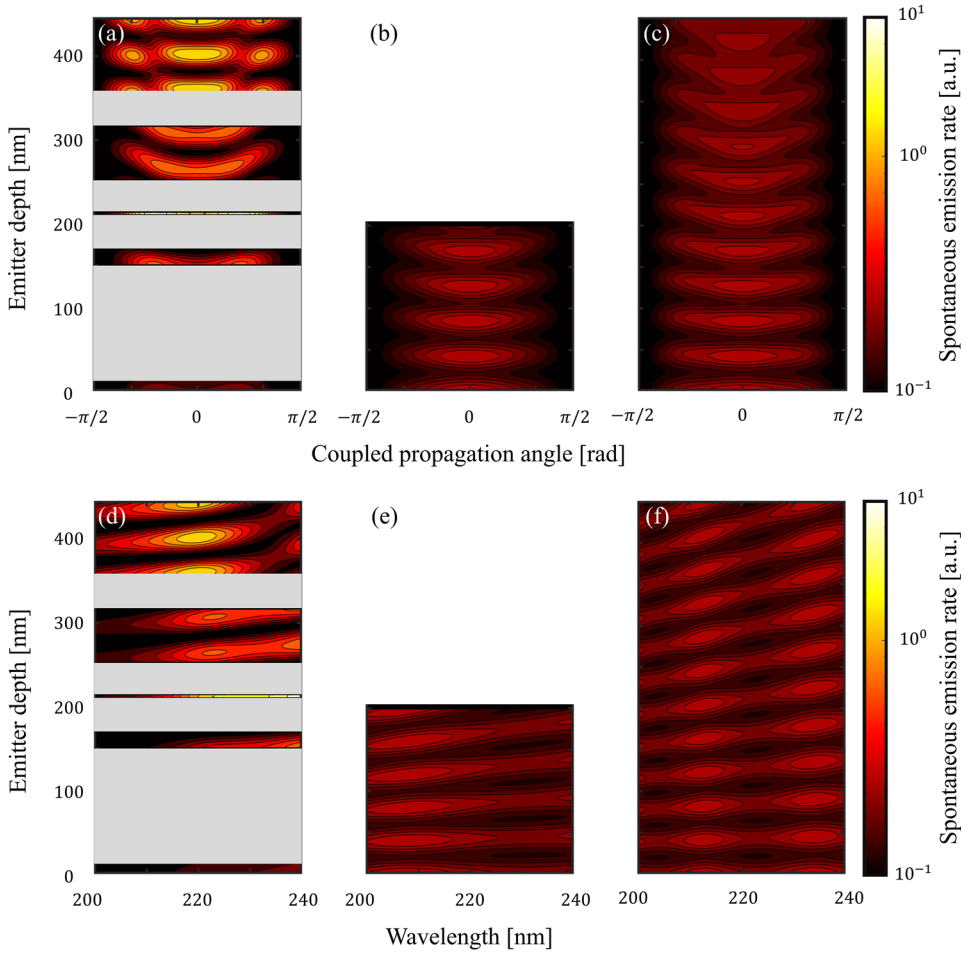

FIG. 2. Spontaneous emission rate dependence on the emitter depth, outcoupling angle, and frequency. (a)–(c) The spontaneous emission rate as a function of depth inside the multilayer structures and outcoupling angle for the optimized structure, and for bulks of thicknesses 200 and 450 nm, respectively. The emission rate is spectrally averaged with the spectral distribution $Y(\omega)$. (d)–(f) The spontaneous emission rate emitted at angle $\theta = 0$, as a function of depth inside the multilayer structures and output light frequency, for the same structures. The non-emitting dielectric layers are marked in gray. All structures are located on a substrate with the refractive index of 1.5. We note that the pattern of emission strongly depends on the structure and on the refractive index of the environment surrounding it (we assume air for the simulations).

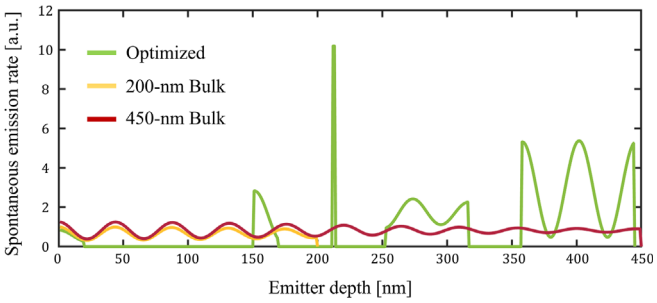

FIG. 3. Spontaneous emission rate dependence on the emitter depth. The spontaneous emission rate as a function of depth inside the multilayer structures for the optimized structure, compared with bulk structures of 200 and 450 nm. The emission rate is averaged over the spectral and angular distributions and is normalized relative to the maximal emission of the 200 nm bulk. The non-emitting dielectric layers in the optimized structure have zero emission. In most of the emitting layers, the emission from the optimized structure is substantially enhanced compared to the bulk structures.

In Eq. (5), z is the depth, $G(z)$ is the emitter spatial distribution at which the input radiation is absorbed before conversion, and $Y(\omega)$ is the emitter's spectral distribution (normalized by $\int Y(\omega)d\omega = 1$). We note that the integrand is non-vanishing only in layers with a phosphor material. The non-emitting dielectric layers only contribute indirectly by altering the optical environment of the phosphor layers.

We design the optimal nanostructure that maximizes the emission's efficiency, by using constrained optimization techniques. More specifically, we define the figure-of-merit of our optimization as the conversion efficiency enhancement (compared to the bulk structure) η:

$$\eta(\boldsymbol{d}) = \frac{\int \sin\theta \mathrm{d}\theta \mathrm{d}\omega\, \Gamma_{\mathrm{eff}}(\theta, \omega; \boldsymbol{d})}{\int \sin\theta \mathrm{d}\theta \mathrm{d}\omega\, \Gamma_{\mathrm{eff,bulk}}(\theta, \omega)}. \tag{6}$$

This figure of merit compares the total outcoupled emission from the nanostructure to the total outcoupled emission of a bulk structure of similar phosphor thickness. We search for the thickness of each individual layer in the structure to reach an optimal performance. To solve the optimization problem and avoid convergence to low maxima, we developed an optimization tool specialized for multilayer photonic design, which relies on the interior-point method.[23] The optimization tool enables us to define complex geometrical constraints, which usually arise from manufacturing limitations. More details can be found in the supplementary material.

To demonstrate the optimization process, Fig. 1(c) illustrates how our optimization tool finds the optimal thicknesses of a structure with two layers. For this specific example, we chose the structure to be a two-layer structure with two degrees of freedom to enable visualizing the optimization map. The result of our optimization for multilayer nanostructures [as illustrated in Fig. 1(b)] is usually aperiodic. Nevertheless, this simple example already shows key features from the more general optimization problem, for instance, that multiple local maxima exist. Moreover, we notice that a 40% enhancement can be achieved for such a photonic crystal structure compared to the naïve bulk structure. We validate our theoretical results with an independent numerical FDTD simulation.

To convert the theoretical equation into practical use, we design a multilayer nanostructure to increase conversion efficiency for a specific phosphor material YPO_4:Pr_3+ (refractive index 2.3)[13] that emits far-UVC light at 235 nm (e.g., by converting 172 nm emitted from a Xe_2 lamp). We form a multilayer structure by combining the phosphor layers with silica layers (refractive index 1.6). Silica is transparent to the input radiation, so no energy is wasted in the dielectric layers. More details about the optical properties of the fused silica that we used can be found in the supplementary material. We analyze thin structures to avoid effects of reabsorption of the emitted UV. Specifically, we compare 200 nm bulk and 450 nm bulk structures to an optimized structure with an overall thickness of 450 nm, of which 200 nm are phosphors. The optimization procedure yields a multilayer with 10 layers, as demonstrated in Fig. 1(b).

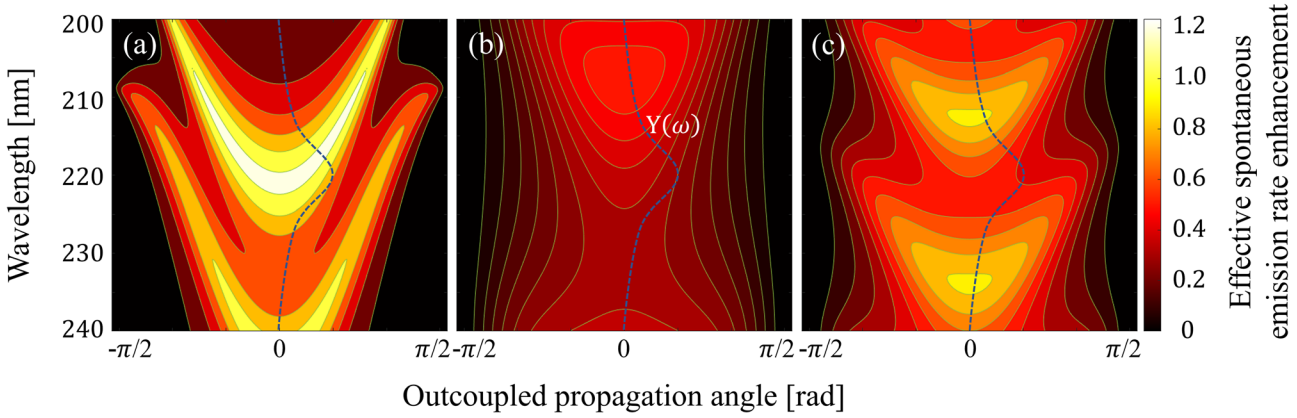

FIG. 4. The phosphor nanostructures emission features. Maps showing the effective spontaneous emission rate enhancement as a function of outcoupling angle θ and wavelength. The emitter's spectral distribution Y(ω) is shown as a dashed blue curve. The maps are normalized such that the effective spontaneous emission of the 200 nm bulk at angle $\theta = 0$ is 1. (a) Map for the optimized structure, where the geometrical characteristics of the structure are optimized to increase the emission into efficiently outcoupled angles and to coincide with the emitters spectral distribution $Y(\omega)$. (b) Map for the 200 nm bulk structure. (c) Map for the 450 nm bulk structure, where there is a mismatch between the points of peak enhancement and the emitters spectral distribution $Y(\omega)$.

In order to analyze the obtained structure's characteristics, we present in Fig. 4 the spontaneous emission rate enhancement for each wavelength and emission angle to free space (θ). The emission rate is calculated according to Eq. (4) and summed over the depth weighted by the absorption profile. Figure 4 emphasizes the role of the structures in shaping the photonic band structure. At each wavelength, the structures increase the emission into some angles and reduce it in other angles. In Figs. 4(a)–4(c), we present the emission map of the optimized structure, 200 and 450 nm bulks, respectively.

Through the optimization process, we enhance the emission into angles that are efficiently outcoupled, while we inhibit the emission into other angles. The optimization matches the spectral regime that is enhanced by the structure such that it coincides with the emitter's spectral distribution $Y(\omega)$ (dashed blue). As a result, the optimized structure's emission features are substantially enhanced compared to those of the bulks, as shown in Fig. 4. For instance, the peak emission at angle $\theta = 0$ is enhanced by factors of 2.4 and 1.4 compared to the 200 and 450 nm bulks, respectively.

Figure 5 shows the angular distribution [Fig. 5(a)] and the temporal signal [Fig. 5(b)] of the optimized structure with 10 layers. In Fig. 5(a), we average the emission rate over the spectrum, weighted by the spectral distribution, to obtain the effective angle-dependent spontaneous emission rate Γ_{eff}. We find that the optimized structure produces more photons at every angle than the 200 nm bulk structure. This effect also arises from reducing emission to angles larger than the critical angle between the phosphor and air. Following Eq. (6), the conversion efficiency is obtained by integrating over the angular distribution, leading to a conversion efficiency enhancement by a factor of 3 compared to the 200 nm bulk. To verify our theoretical findings, we perform numerical FDTD simulations for the emission of the optimized structure (dashed), which show similar enhancements. More details about the FDTD simulations can be found in the supplementary material.

Figure 5(b) presents the comparison between the structures, for the integrated number of emitted photons over time, normalized by a 200 nm bulk phosphor emission.[19] We note that the optimized structure increases the conversion efficiency by a factor of 1.67 compared to a 450 nm bulk phosphor, although it contains only 0.45 of phosphor material. Moreover, the 450 nm bulk phosphor improves the efficiency by a factor of 1.8, although it contains 2.5 more phosphor material. This reveals a fundamental limitation in bulk structures: The conversion efficiency does not scale with the phosphor's thickness. The optimized structure overcomes this limitation. In addition, the time in which the emission occurs is significantly shortened by a factor of 2.5, which can be relevant when considering our approach for other applications [such as optimization of scintillators for Positron Emission Tomography (PET) scans].

Our optimization strategy resulted in highly aperiodic nanostructures, indicating that a naïve approach of a periodic photonic crystal structure is far from optimal, as shown in different works in nanophotonics.[14] It is interesting to consider how the efficiency enhancement depends on the number of layers in the optimized structure. By increasing the number of layers, and as a result the amount of phosphor in the structure, one may expect the efficiency enhancement to saturate due to the increasing absorption in the phosphor layers. However, increasing the number of layers while fixing the total amount of phosphor results in thin layers and deteriorates the Purcell effect. As a result, we expect the optimal structure to have a finite number of layers. Looking forward, our approach can be expanded beyond multilayered structures to 2D and 3D nanostructures. The advantages of our 1D structures are the existence of fabrication methods for layer deposition and the analytical formalism that allows efficient optimization over a large parameter space.

Our results showcase that optimized multilayered nanostructures overcome efficiency limitations of conventional phosphors. As a result, optimizing UV sources through the control of the emission process can impact many applications, from the deactivation of viruses to other medical usages.[2] The optimization tool that we developed can maximize the performance under different figures-of-merit with different parameter constraints.[24] For example, we can improve device lifetimes since the phosphor achieves higher emission power from lower input radiation. Looking at the bigger picture, fundamental sum

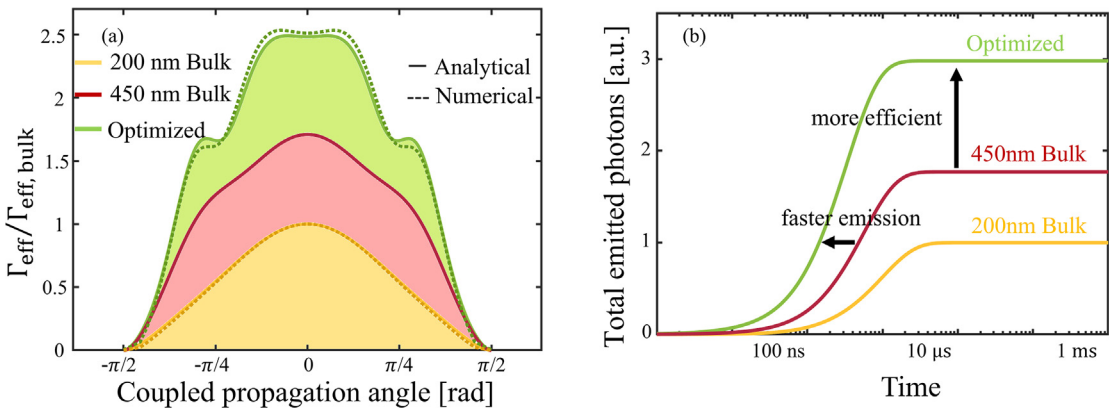

FIG. 5. Optimized multilayered nanostructures for UV emission: enhancement of emission angle, rate, and total photon number. (a) Effective emission rate; comparison of 200 and 450 nm bulk structures (yellow and red curves) and the optimized design (green curves). The emission of the optimized structure is directional due to the LDOS enhancement. The emissions are normalized such that the effective spontaneous emission of the 200 nm bulk at angle $\theta = 0$ is 1. A numerical FDTD simulation (dotted curves) using Lumerical provides additional validation of our analytical framework. (b) The total emitted photons as a function of time, normalized by a 200 nm bulk structure, showing substantial enhancement: by a factor of 3. We also find that the (rise) time of emission is shortened by a factor of 2.5.

rules of the emission process predict that more extensive emission enhancements can be expected, especially for emitters with narrower bandwidths.[25–27] Our approach applies to any material and excitation mechanism, which can be electrical as in LEDs or be emission from excimer lamps.

See the supplementary material for a detailed explanation of the optimization problem, the FDTD simulations, and the optical properties of fused silica at the wavelength of the input radiation.

We thank Professor Gary Eden for the helpful discussions. The research is supported by the GIF Young Scientists' Program and by the Israel Science Foundation (ISF) Grant No. 830/19.

AUTHOR DECLARATIONS

Conflict of Interest

The authors have no conflicts to disclose.

Author Contributions

O.S. and A.S. contributed equally to this work.

DATA AVAILABILITY

The data that support the findings of this study are available from the corresponding author upon reasonable request.

REFERENCES

[1]M. Buonanno, D. Welch, I. Shuryak, and D. J. Brenner, "Far-UVC light efficiently and safely inactivates airborne human coronaviruses," Sci. Rep. **10**, 10285 (2020).
[2]F. J. Garcia de Abajo, R. J. Hernández, I. Kaminer, A. Meyerhans, J. Rosell-Llompart, and T. Sanchez-Elsner, "Back to normal: An old physics route to reduce SARS-CoV-2 transmission in indoor spaces," ACS Nano **14**, 7704 (2020).
[3]M. Raeiszadeh and B. Adeli, "A critical review on ultraviolet disinfection systems against COVID-19 outbreak: Applicability, validation, and safety considerations," ACS Photonics **7**, 2941 (2020).
[4]J. Cadet, "Harmless effects of sterilizing 222-nm far-UV radiation on mouse skin and eye tissues," Photochem. Photobiol. **96**, 949 (2020).
[5]D. A. Laleyan, S. Zhao, S. Y. Woo, H. N. Tran, H. B. Le, T. Szkopek, H. Guo, G. A. Botton, and Z. Mi, "AlN/h-BN heterostructures for Mg dopant-free deep ultraviolet photonics," Nano Lett. **17**, 3738 (2017).
[6]X. Liu, K. Mashooq, D. A. Laleyan, E. T. Reid, and Z. Mi, "AlGaN nanocrystals: Building blocks for efficient ultraviolet optoelectronics," Photonics Res. **7**, B12 (2019).
[7]M. I. Lomaev, V. S. Skakun, É. A. Sosnin, V. F. Tarasenko, D. V. Shitts, and M. V. Erofeev, "Excilamps: Efficient sources of spontaneous UV and VUV radiation," Phys. Usp. **173**, 201 (2003).
[8]W. H. Chiang, D. Mariotti, R. M. Sankaran, J. G. Eden, and K. Ostrikov, "Microplasmas for advanced materials and devices," Adv. Mater. **32**, 1905508 (2020).
[9]J. G. Calvert and J. N. Pitts, *Photochemistry* (Wiley, New York, 1966).
[10]J. Y. Zhang and I. W. Boyd, "Lifetime investigation of excimer UV sources," Appl. Surf. Sci. **168**, 296 (2000).
[11]M. Salvermoser and D. E. Murnick, "Efficient, stable, corona discharge 172 nm xenon excimer light source," J. Appl. Phys. **94**, 3722 (2003).
[12]N. M. Masoud and D. E. Murnick, "High efficiency fluorescent excimer lamps: An alternative to mercury based UVC lamps," Rev. Sci. Instrum. **84**, 123108 (2013).
[13]M. Broxtermann, D. Den Engelsen, G. R. Fern, P. Harris, T. G. Ireland, T. Jüstel, and J. Silver, "Cathodoluminescence and photoluminescence of $YPO_4:Pr^{3+}$, $Y_2SiO_5:Pr^{3+}$, $YBO_3:Pr^{3+}$, and $YPO_4:Bi^{3+}$," ECS J. Solid State Sci. Technol. **6**, R47 (2017).
[14]O. Ilic, P. Bermel, G. Chen, J. D. Joannopoulos, I. Celanovic, and M. Soljačić, "Tailoring high-temperature radiation and the resurrection of the incandescent source," Nat. Nanotechnol. **11**, 320 (2016).
[15]L. Novotny and B. Hecht, *Principle of Nano-Optics* (Cambridge University Press, 2006).
[16]E. M. Purcell, H. C. Torrey, and R. V. Pound, "Resonance absorption by nuclear magnetic moments in a solid," Phys. Rev. **69**, 37 (1946).
[17]E. Yablonovitch, "Inhibited spontaneous emission in solid-state physics and electronics," Phys. Rev. Lett. **58**, 2059 (1987).
[18]D. Kleppner, "Inhibited spontaneous emission," Phys. Rev. Lett. **47**(4), 233 (1981).
[19]Y. Kurman, A. Shultzman, O. Segal, A. Pick, and I. Kaminer, "Photonic-crystal scintillators: Molding the flow of light to enhance x-ray and γ-ray detection," Phys. Rev. Lett. **125**, 040801 (2020).
[20]C. Roques-Carmes, N. Rivera, A. Ghorashi, S. E. Kooi, Y. Yang, Z. Lin, J. Beroz, A. Massuda, J. Sloan, N. Romeo, and Y. Yu, "A general framework for scintillation in nanophotonics," e-print arXiv:2110.11492 (2021).
[21]W. C. Chew, *Waves and Fields in Inhomogenous Media* (Wiley-IEEE Press, 1995), Vol. 16.
[22]J. A. E. Wasey and W. L. Barnes, "Efficiency of spontaneous emission from planar microcavities," J. Mod. Opt. **47**(4), 725 (2000).
[23]S. Wright, *Primal-Dual Interior-Point Methods* (Society for Industrial and Applied Mathematics, 1997).
[24]O. Segal and A. Shultzman, see https://github.com/avners8/Scint_City.git for "Scint City" (2020).
[25]H. Shim, L. Fan, S. G. Johnson, and O. D. Miller, "Fundamental limits to near-field optical response over any bandwidth," Phys. Rev. X **9**, 011043 (2019).
[26]Z. J. Yang, T. J. Antosiewicz, R. Verre, S. P. Apell, F. J. G. D. Abajo, and M. Käll, "Ultimate limit of light extinction by nanophotonic structures," Nano Lett. **15**, 7633 (2015).
[27]O. D. Miller, A. G. Polimeridis, M. T. H. Reid, C. W. Hsu, B. G. DeLacy, J. D. Joannopoulos, M. Soljacič, and S. G. Johnson, "Fundamental limits to optical response in absorptive systems," Opt. Express **24**, 3329 (2016).